JOURNAL OF SOLID STATE CHEMISTRY **124,** 17–23 (1996)
ARTICLE NO. 0201

$CuYb_2Ge_4O_{12}$, a New Bidimensionally Tunneled Structure

J. A. Campá,* C. Cascales,† E. Gutiérrez-Puebla,† M. A. Monge,† I. Rasines,†,[1] and C. Ruíz Valero†

*Facultad de Ciencias Geológicas, Universidad Complutense de Madrid, 28040 Madrid, Spain; and †Instituto de Ciencia de Materiales, CSIC, Cantoblanco, 28049, Madrid, Spain

Received September 13, 1995; in revised form February 19, 1996; accepted February 21, 1996

Employing CuO as self flux crystals of $CuYb_2Ge_4O_{12}$ have been grown for the first time. The crystal structure of $CuYb_2Ge_4O_{12}$ has been determined by single-crystal X-ray diffraction in the triclinic $P\bar{1}$ (No. 2) space group to an R value of 6.1%, with $a = 7.156(2)$ Å, $b = 7.937(3)$ Å, $c = 4.905(3)$ Å, $\alpha = 86.63(3)°$, $\beta = 102.41(4)°$, $\gamma = 114.12(3)°$, $V = 248.2(2)$ Å^3, $Z = 1$, and $D_c = 5.97$ gcm^{-3}. The novel tridimensional $CuYb_2Ge_4O_{12}$ structure type can be conceived as formed by layers of $(GeO_4)_4$ units of vertex-sharing GeO_4 tetrahedra, chains of YbO_7 polyhedra, and isolated CuO_4 squares connecting $(GeO_4)_4$ units, with channels or tunnels of size up to 4.08 Å in the a and c directions. A comparison is made between the structure types of the title germanate and recently reported $CuNd_2Ge_2O_8$. The temperature dependence from 350 to 1.8 K of the reciprocal dc magnetic susceptibility for $CuYb_2Ge_4O_{12}$ is shown and presents a deviation from linearity over the whole temperature range. The infrared spectrum between 1000 and 100 cm^{-1} is given and related with those of comparable species. © 1996 Academic Press, Inc.

I. INTRODUCTION

The possibility of obtaining self-activated crystals in which a good number of interesting optical effects can be found led in the eighties to the study of rare-earth, R, germanates containing Al, Ga, or Fe, which show the monoclinic $RAlGe_2O_7$ structure type (1). Similar effects could be found in crystals of rare-earth germanates in which Al was replaced by a 3d divalent metal of similar size. In particular, the study of oxides characterized by a mixed framework built up from GeO_4 tetrahedra (rarely GeO_5 trigonal bipyramids), planar CuO_4 squares, and RO_n polyhedra seemed to us very attractive due to the possibility of original physical properties for such materials. We have recently (2) grown crystals of $CuNd_2Ge_2O_8$, establishing a new structural type for the $CuR_2Ge_2O_8$ (R = Y, La–Yb) family. Although all the possible examples of this kind of systems consist of similar basic units, as a function of the stoichiometry they can show considerable variety in their polyhedra connectivities, with linkages involving Ge–O–Ge, Cu–O–Cu, and Ge–O–Cu bonds, as well as different coordination RO_n polyhedra for the involved rare earth. In this paper we report another result of our exploratory synthesis and crystal growth in the R–Ge–Cu–O system: a member, R = Yb, of the $CuR_2Ge_4O_{12}$ (R = Y, Eu–Lu) family (3), which defines a new structure type. The measurement of some properties of $CuYb_2Ge_4O_{12}$ is also reported.

[1] To whom correspondence is to be addressed.

II. EXPERIMENTAL DETAILS

Crystal growth. A good number of our previous attempts at growing crystals of the title compound showed the deep influence of the flux employed in order to avoid the high viscosity of the melts containing GeO_2. Nominal compositions near $CuYb_2Ge_4O_{12}$ in the absence of the right flux led to massive nucleation and to agglomerates of microcrystals showing an aplitic structure. Mixtures with relatively high contents of GeO_2, CuO, and the adequate flux gave small $CuYb_2Ge_4O_{12}$ single crystals. Those used for this work were grown from mixtures of reagent-grade CuO, Yb_2O_3, and GeO_2 at Cu : Yb : Ge = 2 : 2 : 5 molar ratios using Bi_2O_3 as a flux in platinum crucibles. These mixtures were heated to 1250°C, soaked for 45 min, and cooled to 1055°C at the rate of 4°C hr^{-1} and subsequently to room temperature after turning the power off. After the excess of flux was completely removed with dilute nitric acid, the resulting mass was filtered, dried, and identified as a mixture of single crystals of $CuYb_2Ge_4O_{12}$, GeO_2, and $CuGeO_3$, which were characterized by energy dispersive X-ray analysis and X-ray powder diffraction as indicated elsewhere (4). Crystals identified (3, 5) as $CuYb_2Ge_4O_{12}$ could be isolated using 30% HCl, which dissolves CuO and $CuGeO_3$ and does not attack $CuYb_2Ge_4O_{12}$ crystals.

X-ray structure determination. A greenish blue $CuYb_2Ge_4O_{12}$ crystal showing not very well defined faces was mounted in a kappa diffractometer. A summary of its fundamental data is given in Table 1. The cell dimensions were refined by least squares fitting the θ values of 25 reflections. The intensities were corrected for Lorentz and

0022-4596/96 $18.00

TABLE 1
Crystal and Refinement Data for $CuYb_2Ge_4O_{12}$

Formula	$CuYb_2Ge_4O_{12}$
Formula wt	892.0
Crystal system	triclinic
Space group	$P\bar{1}$ (No. 2)
Cell dimensions	
a, Å	7.156(2)
b, Å	7.937(3)
c, Å	4.905(3)
α, °	86.63(3)
β, °	102.41(4)
γ, °	114.12(3)
Z	1
V, Å^3	248.2(2)
D_{calcd}, g cm^{-3}	5.97
$F(000)$	393
Temp, °C	22
Diffractometer	Enraf–Nonius
Radiation	graphite monochromated Mo$K\alpha$ (λ = 0.71069 Å)
μ(Mo$K\alpha$), cm^{-1}	326
Crystal dimensions, mm	0.15 × 0.15 × 0.05
θ range, °	1–30
Scan technique	$\omega/2\theta$
Scan speed range, ° min^{-1}	1.83–16.48
Data collected	(−10, −11, 0) to (10, 11, 11)
Unique data	1439
Observed reflections $I > 2\sigma(I)$	1312
Decay	≤1%
R_{int}, %	5.0
Standard reflections	1/27
$R = \sum \lvert\Delta F\rvert / \sum \lvert F_o\rvert$	6.1
$R_w = (\sum w\Delta F^2 / \sum w \lvert F_o\rvert^2)^{1/2}$	8.6
Average shift/error	0.3
Absorption correction range	0.739–1.520

polarization effects. Scattering factors for neutral atoms and anomalous dispersion corrections for Cu, Ge, and Yb were taken from the International Tables for X-Ray Crystallography (6). The structure was solved by Multan and Fourier methods. The centrosymmetric $P\bar{1}$ space group was obtained during the course of the structure solution. An empirical absorption correction (7) was applied at the end of the isotropic refinement. Mixed full-matrix least-squares refinements were performed minimizing $\sum w(\lvert F_o\rvert - \lvert F_c\rvert)^2$ with unit weights and led to the R value of 0.061. Final difference synthesis showed no significant electron density. Most of the calculations were carried out with the X-Ray 76 system (8).

Spectroscopic studies. A FT-IR Nicolet SX60 spectrometer was used in the range 1000–100 cm^{-1} with powdered samples dispersed either in KBr or polyethylene pellets.

Magnetic measurements. A SQUID magnetometer (Quantum Design) operating from 350 to 1.8 K under zero-field cooling conditions at 1000 and 10 Oe, was used to perform dc magnetic measurements on $CuYb_2Ge_4O_{12}$ single crystals. Diamagnetic corrections (9) for the magnetic susceptibilties were taken into account.

III. RESULTS

$CuYb_2Ge_4O_{12}$ crystals were small, about 0.2 mm in size, transparent, and greenish blue colored. Although they appeared as elongated prisms, they were formed by a combination of three pinacoids. Their unit-cell dimensions are given in Table 1. Atomic position coordinates and thermal parameters as well as main interatomic distances and angles are included in Tables 2 and 3.

Both Ge atoms in $CuYb_2Ge_4O_{12}$ exhibit the usual tetrahedral coordination, with distances and angles similar to those found in $CuGeO_3$ (10). Cu atoms are situated in inversion centers with planar square oxygen coordination. However, some kind of interaction with O3 atoms is present, since Cu–O3 distances are 2.71(2), as in $CuGeO_3$ (10). Yb atoms are seven-coordinated. Table 4 shows the planarity study around the Yb atom. Taking into account the geometrical criteria given for idealized polytopal forms (11) as well as the results of our planarity study, we conclude that the shape of the YbO_7 polyhedron is close to a C_{3v} capped octahedron. The five atoms in equal positions (O2, O5, O4, O6′, and Yb) form a plane, with a maximum deviation of 0.09(1) Å. The YbO_6 octahedra of Fig. 1 are

TABLE 2
Atomic Coordinates and Thermal Parameters for $CuYb_2Ge_4O_{12}$

Atom	x/a	y/b	z/c	U_{eq}
Yb	0.2285(1)	0.4491(1)	0.0364(2)	17(3)
Ge1	0.3815(3)	0.2062(3)	−0.4223(4)	36(7)
Ge2	0.1674(3)	0.7787(3)	−0.4568(4)	36(7)
Cu	0.0000(0)	0.0000(0)	0.0000(0)	64(11)
O1	0.2207(25)	0.1926(23)	−0.7472(34)	91(28)
O2	−0.0059(24)	0.7961(22)	−0.7521(32)	60(49)
O3	0.2882(26)	−0.0066(23)	−0.2739(35)	103(56)
O4	0.3526(30)	0.7228(27)	0.4257(39)	158(34)
O5	0.4270(26)	0.3939(24)	−0.2162(35)	102(54)
O6	0.0604(26)	0.6108(23)	−0.2336(34)	99(53)

Atom	U_{11}	U_{22}	U_{33}	U_{12}	U_{13}	U_{23}
Yb	9(4)	16(4)	26(4)	3(3)	8(3)	1(3)
Ge1	28(9)	23(9)	43(9)	4(7)	−14(7)	−7(7)
Ge2	32(9)	16(9)	48(9)	3(7)	−1(7)	10(7)
Cu	76(16)	10(14)	55(15)	−5(12)	−42(12)	−3(12)
O1	91(28)					
O2	70(65)	78(66)	50(66)	59(54)	−19(52)	−30(52)
O3	80(75)	81(77)	150(72)	3(62)	102(59)	25(60)
O4	158(34)					
O5	100(72)	90(72)	122(71)	21(60)	53(58)	−78(57)
O6	41(71)	32(72)	182(71)	−4(59)	−30(57)	−26(57)

Note. $U_{eq} = \frac{1}{3} \sum_i \sum_j U_{ij} a_i * a_j * \mathbf{a}_i \cdot \mathbf{a}_j \times 10^4$.

TABLE 3
Interatomic Distances (Å) and Angles (°)

Yb–O4	2.71	Ge1–O5	1.73
Yb–O5	2.25	Ge1–O4	1.75
Yb–O6	2.29	Ge2–O2	1.73
Yb–O1	2.23	Ge2–O3	1.75
Yb–O5	2.26	Ge2–O4	1.76
Yb–O6	2.33	Ge2–O6	1.71
Yb–O2	2.26	Cu–O1	1.94 × 2
Ge1–O1	1.73	Cu–O2	1.96 × 2
Ge1–O3	1.72	Cu–O3	2.71 × 2
O1–Ge1–O3	108.10	O4–Ge2–O6	106.6
O1–Ge1–O4	114.9	O1–Cu–O2	95.6 × 2
O1–Ge1–O5	113.95	O1–Cu–O2	84.4 × 2
O3–Ge1–O4	110.2	O1–Cu–O3	89.6 × 2
O3–Ge1–O5	116.07	O1–Cu–O3	90.4 × 2
O4–Ge1–O5	93.2	O1–Cu–O1	180.0
O2–Ge2–O3	108.2	O2–Cu–O2	180.0
O2–Ge2–O4	106.7	O2–Cu–O3	97.6 × 2
O2–Ge2–O6	115.58	O2–Cu–O3	82.4 × 2
O3–Ge2–O4	111.2	O3–Cu–O3	180.0
O3–Ge2–O6	108.7		

Note. Average esd's 0.02 (Å) and 0.8 (°).

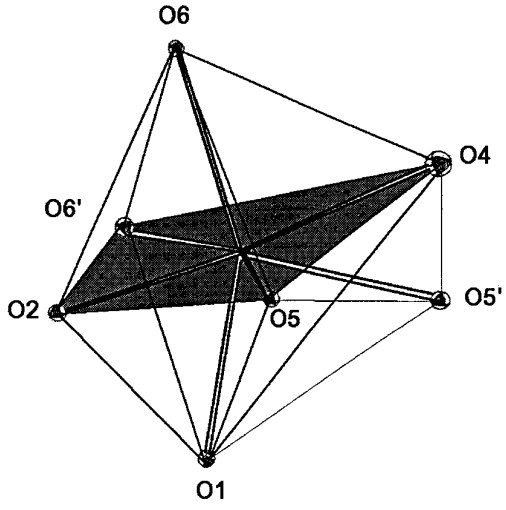

FIG. 1. YbO_7 coordination polyhedra in $CuYb_2Ge_4O_{12}$. Shadowed area corresponds to the calculated equatorial plane (E.P.) given in Table 4.

capped by the O5′ atom on the face defined by the O1, O4, and O5 atoms. The dihedral u_1, u_2, and u_3 angles of Table 4 which correspond to the capped face of the octahedron have values (°) of 21.4(8), 32.6(8), and 23.5(5), close to those given in the literature (11) for the C_{3v} model in ideal ML_7 polyhedra ($u_1 = u_2 = u_3 = 24.2°$).

Every four GeO_4 tetrahedra are associated by sharing vertices forming tetrameric $(GeO_4)_4$ units. On these associations it is worth to point out that those germanate groups joined through the O3 atom (Ge1–O3–Ge2) are arranged in an eclipsed configuration; and for O4 as common vertex (Ge1–O4–Ge2) the alternate configuration occurs. As it will be shown, $(GeO_4)_4$ tetramers play an important role in the structure, which can be conceived as formed by layers of $(GeO_4)_4$ tetramers of vertex sharing GeO_4 tetrahedra parallel to the **ab** plane. As can be seen in Figs. 2 and 3, there is no direct joining between tetrameric units. Never-

TABLE 4
Angles (°) between Principal Planes and Apical Line (A.L.) in YbO_7 Polyhedron

E.P.	O2–O4–O5–O6′	A.L.	O1–O6
P.1	O6–O2–O6′	P.8	O1–O4–O6′
P.2	O6–O4–O6′	P.9	O5′–O4–O5
P.3	O6–O4–O5	P.10	O5′–O1–O5
P.4	O6–O2–O5	P.11	O5′–O4–O1
P.5	O1–O4–O5	P.12	O5′–O5–O2
P.6	O1–O2–O5	P.13	O5′–O4–O6′
P.7	O1–O2–O6′		
E.P. ∧ A.L.	77.2(4)	P.4 ∧ P.8	14.0(6)
P.1 ∧ P.5	12.5(7)	P.3 ∧ P.9 = u_1	21.4(8)
P.2 ∧ P.6	21.8(6)	P.10 ∧ P.12 = u_2	32.6(8)
P.3 ∧ P.7	8.1(6)	P.11 ∧ P.13 = u_3	23.5(5)

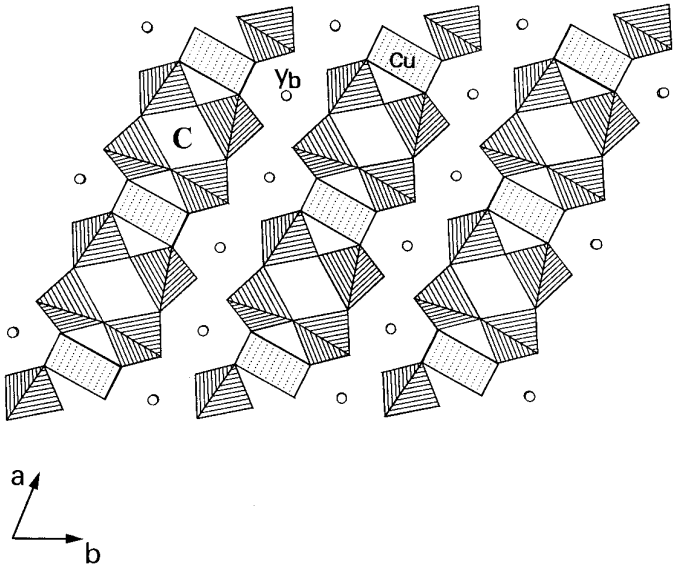

FIG. 2. View of the lattice of $CuYb_2Ge_4O_{12}$ along the **c** direction. Tetrameric $(GeO_4)_4$ units are formed by alternate $Ge1O_4$ and $Ge2O_4$ tetrahedra.

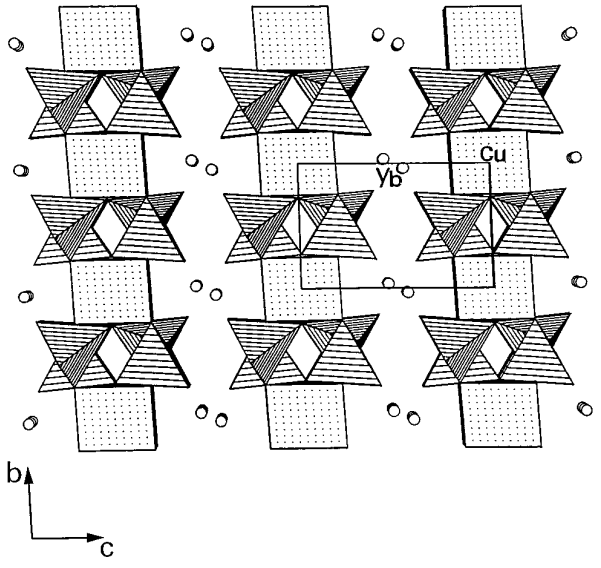

FIG. 3. View of the lattice of $CuYb_2Ge_4O_{12}$ along the **a** direction.

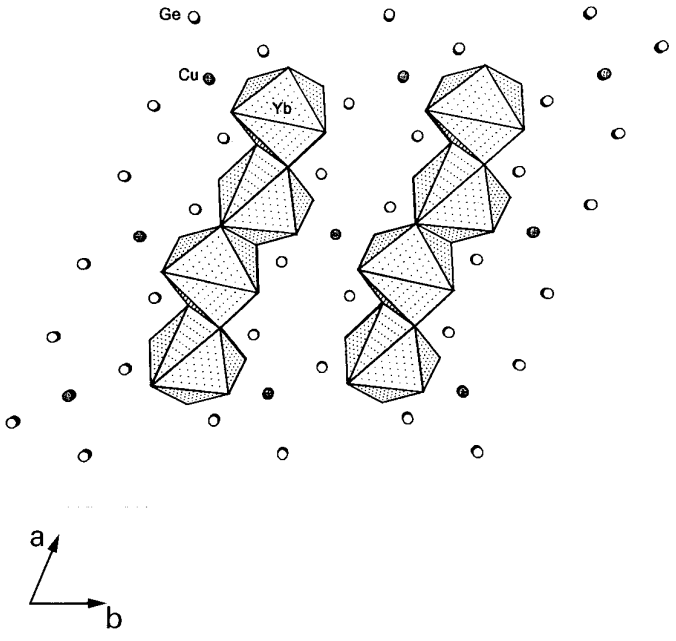

FIG. 5. YbO_7 polyhedra chains in the [100] direction.

theless, in the **c** direction, isolated CuO_4 squares connect $(GeO_4)_4$ units by sharing O2 and O1 vertices with two different GeO_4 tetrahedra, as Fig. 4 shows. YbO_7 polyhedra form chains parallel to the **a** direction (Fig. 5) by sharing the O5–O5′ and O6–O6′ edges with the two up and down neighbor polyhedra, respectively. In the **b** direction these YbO_7 chains are connected through $(GeO_4)_4$ units and CuO_4 squares by sharing the O4–O5 edge and the O5 and O1 vertices with different Ge1 tetrahedra. O6 and O2 vertices and the O4–O6 edge are shared with different Ge2 tetrahedra too, and the O1, O2 vertices with Cu squares.

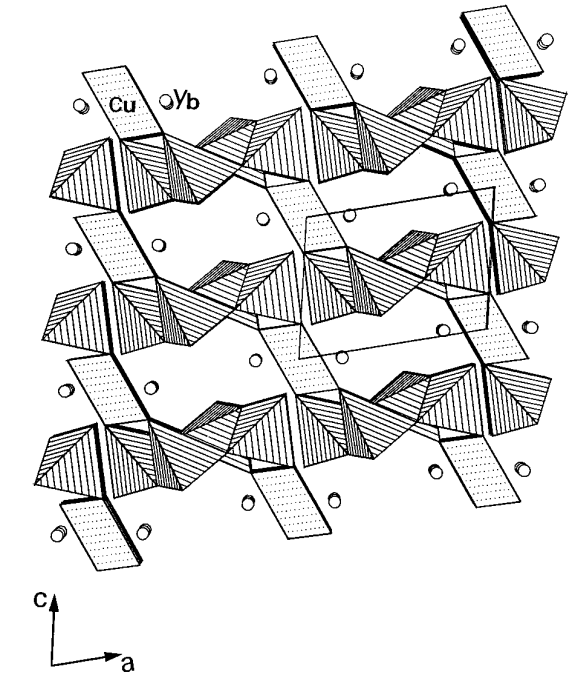

FIG. 4. View of the lattice of $CuYb_2Ge_4O_{12}$ along the **b** direction, showing connections between tetrameric $[(GeO_4)_4]_n$ layers through CuO_4 squares.

This 3D structure contains three types of tunnels, the tetrameric $(GeO_4)_4$ units being involved in all of them. Those labeled as C in Fig. 2 and hereafter are formed along **c** because of the holes created in the middle of the tetramers. These C tunnels are centered at $(\frac{1}{2}, 0, z,)$ and cross $[(GeO_4)_4]_n$ layers. The shape and size of the corresponding four-ring window (as viewed along the **c** axis) is drawn in Fig. 6a.

In the **a** direction two kinds of tunnels, A1 and A2, are formed. A1 is centered at $(x, \frac{1}{2}, \frac{1}{2})$ and A2 at $(x, 0, \frac{1}{2})$, as shown in Fig. 7. A1 is built up from two YbO_7 polyhedra and two GeO_4 tetrahedra, but in fact these polyhedra are helically arranged. This means that, strictly speaking, the window of this channel is not a real ring. On the other hand, due to the different GeO_4 polyhedron configurations in the tetramers above mentioned, every two consecutive ''windows'' along the **a** direction are mutually shifted in the **b** direction, in such a way that A1 tunnels run zig-zag along [100], like the two chains of $(YbO_7)_n$ polyhedra situated up and down. Figure 6b shows the shape and size of the A1 rings as viewed along the **a**-axis. The smallest A2 tunnels are only a consequence of the tetrameric association of the germanate groups. As A2 intersects with the C channel, the intersection between C and A1 is avoided by the O4 atom.

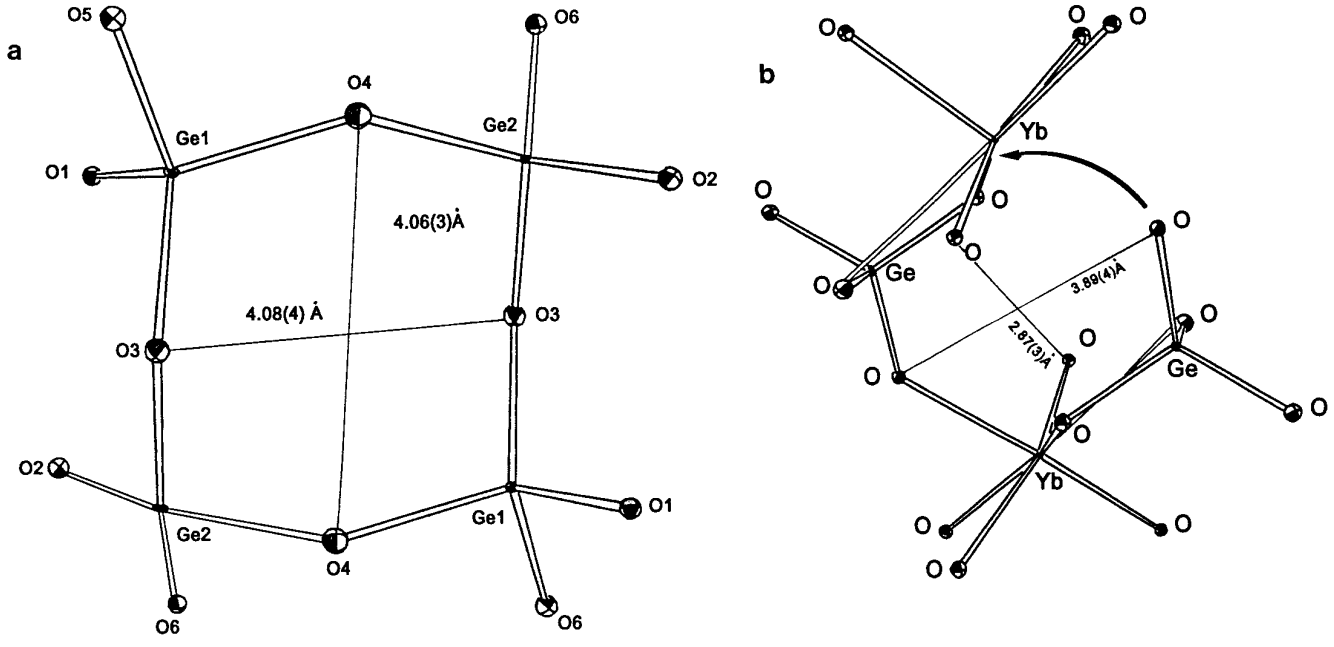

FIG. 6. ORTEP view of the shape and size of the free windows corresponding to C in (a) and A1 in (b) tunnels present in the structure of $CuYb_2Ge_4O_{12}$.

Looking at the coordination polyhedra present in each case, a number of differences have been found between the $CuNd_2Ge_2O_8$ structure type (I), recently (2) reported by us, and that of $CuYb_2Ge_4O_{12}$ (II). I and II contain CuO_6 octahedra and CuO_4 squares, respectively. All Ge polyhedra in II are regular tetrahedra, whereas I shows two kind of coordinations, GeO_5 trigonal bipyramids and rather regular GeO_4 tetrahedra. As for the rare earth, even the coordination number is different: in I the rare earth is coordinated to eight oxygens forming D_{2d} triangulated dodecahedra, and RO_7 C_{3v}-capped octahedra are present in II. With regard to polyhedral connectivities, two features are noteworthy. The rare earth forms sharing-edges tetrameric $(RO_8)_4$ units in I and (RO_7) chains in II. CuO_6 chains exist in I, but not in II, where each CuO_4 connects two different $(GeO_4)_4$ tetrameric units in such a way that connectivities change from O–Cu–O–Cu–O in I to Cu–O–Ge–O–Ge–O–Cu in II. Although the unit-cell volume per oxygen atom is almost identical in I and II, 20.6 and 20.7 $Å^3$ respectively, the differences mentioned indicate that in $CuR_2Ge_4O_{12}$ we have obtained a more open structure type showing intersecting channels that make it an interesting material as a substrate possibly adequate for Li or H intercalation reactions.

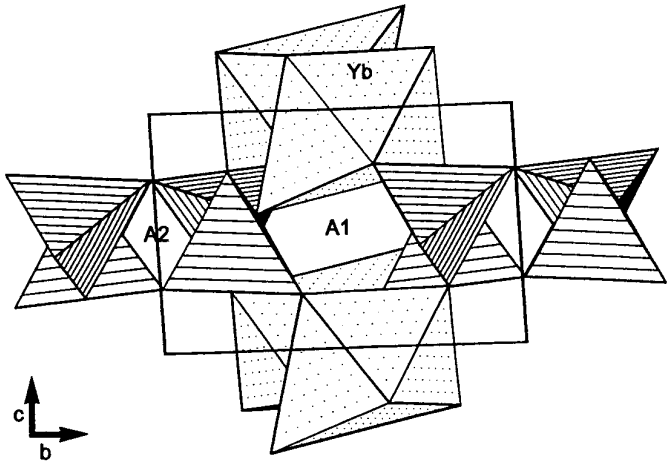

FIG. 7. View of the lattice of $CuYb_2Ge_4O_{12}$ along [100], without CuO_4 squares, showing A1 and A2 tunnels.

The characteristic IR absorptions are shown in Fig. 8. Although the detailed assignment of that complex spectrum is not possible within the purpose of our work, some conclusions can be drawn. It is clear that most of the bands in spectral ranges $\sim 900\ cm^{-1}$, $\sim 800\ cm^{-1}$, and $\sim 500\ cm^{-1}$ can be related (12) to the stretching vibrations ν_{as} at 859 cm^{-1}, $\nu(Ge = O)$ at 770–720 cm^{-1}, and ν_s at 625–533 cm^{-1} of the GeO_4 groups at $CuGeO_3$. A parallel assignment can be found for three GeO_2 inclusion compounds (13) whose frameworks consist mainly of GeO_4 tetrahedra, and two Nd germanates, Nd_2GeO_5 and Nd_3GePO_9, that contain GeO_4 tetrahedra too (14). The vibrations in the wavenumber range 600–350 cm^{-1} are fairly complex. A contribution to most of them is probably made not only by the lanthanide–oxygen bond stretching coordinates but also by the

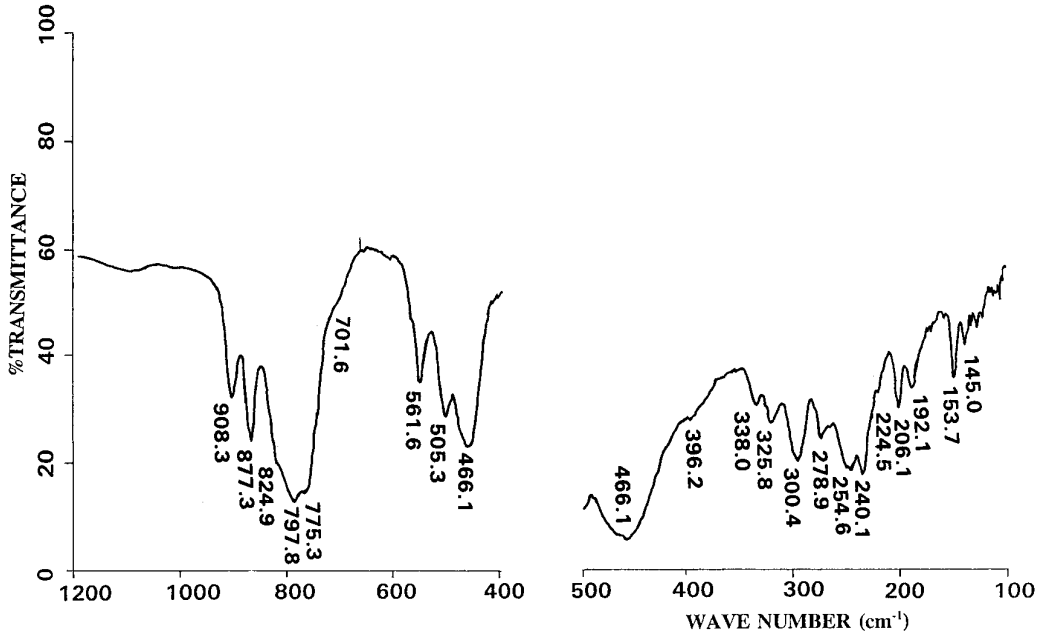

FIG. 8. Infrared spectrum of $CuYb_2Ge_4O_{12}$.

Cu-squares stretching, as indicated (15) for a series of mixed rare-earth copper oxides, $NdRCuO_4$ (R = La, Nd, Sm, Ge, Dy). The strong vibrations found at 505–466 cm^{-1} would be assigned to ν (Yb–O; Cu–O) modes, whereas vibrations at 338–326 cm^{-1} could be attributed to υ(Yb–O) modes. The wavenumbers below 326 cm^{-1} may be due to the bending vibrations of the different coordination polyhedra present in $CuYb_2Ge_4O_{12}$: δ(Ge–O) modes are reported at 332 cm^{-1} for hexagonal GeO_2 (16) and δ(O–R–O) lying between 320 and 210 cm^{-1} for the above-mentioned (15) mixed rare-earth copper oxides.

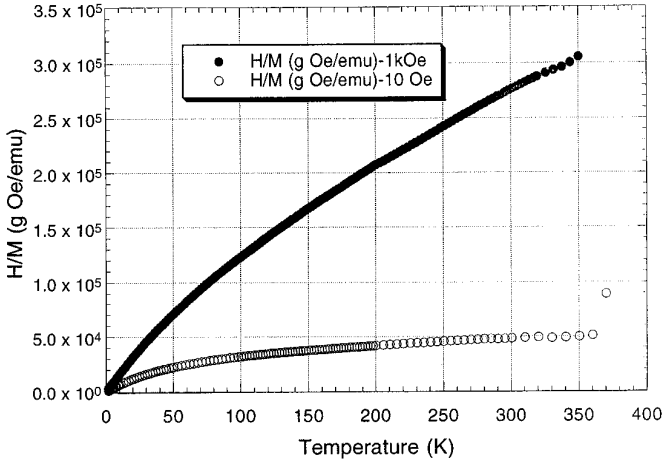

FIG. 9. Reciprocal of the dc magnetic susceptibility of $CuYb_2Ge_4O_{12}$ as a function of the temperature.

The temperature dependence of the reciprocal magnetic susceptibility, χ^{-1}, for $CuYb_2Ge_4O_{12}$ at 1000 Oe is shown in Fig. 9. As it can be observed, the plot presents a deviation from linearity over the whole temperature range. This effect looks slight in the range 75–350 K and stronger below 75 K. In the indicated range of temperatures $CuYb_2Ge_4O_{12}$ does not follow Curie–Weiss behavior. Since no maxima in χ are observed at low temperatures, it is clear that under 75 K the effect of the crystal-field splitting of the $^2F_{7/2}$ ground state for Yb^{3+} is responsible of the downward deviation from linearity in the χ^{-1} vs T plot. Often this deviation has been erroneously attributed to cooperative magnetic interactions. Effectively, it is observed in other Yb compounds (17–19) in which this kind of magnetic interaction is not present. On the other hand, when a possible antiferromagnetic ordering is expected at relatively low temperatures, as could be the present case, T_N is a function of the applied magnetic field and the antiferromagnetic ordering can easily be perturbed by an excessively strong magnetic field. Measurements made at 10 Oe (Fig. 9) did not detect any maximum in χ vs T. This indicates that the antiferromagnetic ordering for the rare-earth sublattice is not completely reached, but the observed reduction in the magnetic moment when the temperature decreases could be justified by some ordering gradually induced by the polarization of the Cu^{2+} ions, as was found and explained (20) for $BaCuYb_2O_5$.

ACKNOWLEDGMENTS

This work was supported by the Comisión Interministerial de Ciencia y Tecnología under Project PB94-0031. The authors gratefully acknowledge

the assistance of J. L. Martínez, who made the magnetic measurements, and the helpful comments of J. Marco.

REFERENCES

1. A. A. Kaminskii, B. V. Mill, A. V. Butashin, E. L. Belokoneva, and K. Kurbanov, *Phys. Status Solidi* (*a*) **103,** 575 (1987).
2. J. A. Campá, E. Gutiérrez Puebla, M. A. Monge, C. Ruíz Valero, C. Cascales, and I. Rasines, *J. Solid State Chem.* **120,** 254 (1995).
3. U. Lambert and W. Eysel, *Powder Diffr.* **1,** 256 (1986).
4. J. A. Campá, E. Gutiérrez-Puebla, M. A. Monge, I. Rasines, and C. Ruíz Valero, *J. Cryst. Growth* **125,** 17 (1992).
5. Powder Diffraction File, Card No. 37-1353. International Centre for Diffraction Data, Swarthmore, PA.
6. J. A. Ibers and W. C. Hamilton (Eds.), ''International Tables for X-Ray Crystallography,'' Vol. IV, pp. 79, 80, and 90, Kynoch, Birmingham, 1974.
7. N. Walker and D. Stuart, *Acta Crystallogr. Sect. A* **39,** 158 (1983).
8. J. M. Stewart, P. A. Machin, C. W. Dickinson, H. L. Ammon, H. Heck, and H. Flack, ''The X-ray 76 System.'' Technical Report TR-446, Computer Science Center, University of Maryland, College Park, MD, 1976.
9. Ch. J. O'Connor, *in* ''Progress in Inorganic Chemistry,'' (S. J. Lippard, Ed.), Vol. 29, p. 210. Wiley, New York, 1982.
10. H. Völlenkle, A. Wittmann, and H. Nowotny, *Monatsh. Chem.* **98,** 1352 (1967).
11. E. L. Muetterties and L. J. Guggenberger, *J. Am. Chem. Soc.* **96,** 1748 (1974).
12. D. M. Adams and P. A. Fletcher, *Spectrochim. Acta Part A* **44,** 233 (1988).
13. J. Cheng, R. Xu, and G. Yang, *J. Chem. Soc. Dalton Trans.,* 1537 (1991).
14. B. F. Dzhurinskii, I. V. Tananaev, E. G. Tselebrovskaya, and A. I. Prozorovskii, *Izv. Akad. Nauk SSSR Neorgan. Mater.* **27,** 255 (1991).
15. V. B. Lazarev and I. S. Shaplygin, *Russ. J. Inorg. Chem.* **26,** 947 (1981).
16. E. R. Lippincott, A. Van Valkenburg, C. E. Weir, and E. N. Bunting, *J. Res. Natl. Bur. Stand.* **61,** 61 (1958).
17. F. Fernández, R. Sáez Puche, C. Cascales, C. M. Marcano, and I. Rasines, *J. Phys. Chem. Solids* **50,** 871 (1989).
18. M. D. Guo, A. T. Aldred, and S. K. Chan, *J. Phys. Chem. Solids* **48,** 229 (1987).
19. C. Cascales, R. Sáez-Puche and P. Porcher, *J. Phys. Condens. Matter,* to appear.
20. A. J. Salinas-Sánchez, Ph.D. Thesis. Universidad Complutense de Madrid, Madrid, 1992.